Correlation between mechanical scales and analysis scales of topographic signals under milling process of natural fibre composites

Faissal Chegdani, Sabeur Mezghani and Mohamed El Mansori

Abstract

This article aims to find the relation between the multiscale mechanical structure of natural fibre reinforced plastic composites and the analysis scales in the topographic signals of machined surfaces as induced by profile milling process. Bamboo, sisal and miscanthus fibres reinforced polypropylene composites were considered in this study. The multiscale process signature of natural fibre reinforced plastic machined surfaces based on wavelet decomposition was determined. Then, the impact of wavelet function was inspected by testing different wavelet shapes. Finally, the analysis of variance was carried out to exhibit the contribution rate of fibre stiffness and tool feed on the machined surface roughness at each analysis scale. Results demonstrate that studying the machining of natural fibre reinforced plastic requires the selection of the relevant scales. They show also the insignificance of the wavelet choice. This study proves that the contribution rate of fibre stiffness and tool feed on machined surface roughness is significantly dependent on the analysis scales, which are directly related to the mechanical properties of natural fibres structure inside the composite.

Keywords

Natural fibre composites, multiscale signal topography, discrete wavelet transform, analysis of variance, profile milling process, surface roughness

Introduction

The use of natural fibres as reinforcement in plastic composites has raised the interest of academia and industry thanks to their higher mechanical properties compared with their low weight in addition to their economic and ecological benefits.[1–4] Apart from their low production cost, the use of natural fibres is justified by the valorization of local resources and the enhancement of materials and technologies taking into account the environmental impacts and the sustainable development.[5,6]

Profile milling is the unavoidable machining step required for achieving the surfaces of final products.[7] Thus, machining surface state has to be analysed in order to evaluate the efficiency of profile milling process. However, and because of heterogeneity in the internal structure of fibre reinforced plastic composites, usual surface roughness characterization parameters from ISO 4287 such as standard arithmetical roughness average (R_a) are not adapted to reliably characterize the surface quality on composites.[8]

Multiscale decomposition method of surface topography is suitable in the case of complex surface topography, where the signal contains discontinuities and sharp peaks, since it takes into account all the scales of decomposition without any cut-off.[9] It is based on wavelets transform, which are a kind of mathematical function that cut up data into different frequency components and then study each surface component with a resolution matched to its scale.[10] This allows the determination of the multiscale transfer function of the morphological modification on surface topography as induced by the machining process. This multiscale approach has been successfully applied to analyse machining surfaces obtained by belt-finishing and

Arts et Métiers ParisTech, MSMP – EA7350, France

Corresponding author:
Faissal Chegdani, Arts et Métiers ParisTech, MSMP – EA7350, Rue Saint Dominique, BP 508, 51006, Châlons-en-Champagne, Cedex, France.
Email: faissal.chegdani@ensam.eu

honing processes.[11] It was also demonstrated that the wavelet approach is useful when characterizing localized surface defects while Gaussian filtering is more appropriate for highly periodic morphological structures.[12]

Nevertheless, this approach involves the choice of the wavelet analysis method (discrete or continuous transform) and the choice of wavelet function shape. This can have significant effect on the analysis results depending on the studied manufacturing process or engineering surfaces application.[13] In fact, for honing process, it has been demonstrated that the regularity property of wavelet function has a significant influence on the characterization of its industrial performances.[14] However, the morphological changes of surfaces generated by belt-finishing process and characterized by several surface parameters are statistically similar regardless the shape of the wavelets.[15]

The multiscale approach based on 1D discrete wavelet transform (DWT) has been first introduced in Chegdani et al.[16] to analyse the natural fibre reinforced plastic (NFRP) surfaces machined by profile milling process. The results have shown that the qualities of the milled NFRP surfaces are significantly dependent on fibre stiffness at the fibre bundle section scales. In this article, the contribution rate of material and processing effects (i.e. natural fibre stiffness and cutting tool feed) was evaluated at each scale of the NFRP machined surface quality. The characteristic scales for the analysis of both fibre stiffness and tool feed influence on the milled surface roughness have been determined by calculating the multiscale process signature (MPS) at each profile milling configuration. Various wavelet functions are considered for the surface characterization of the milled NFRP topographic profiles in order to highlight the effect of the wavelet function choice. The sensitivity of wavelet function shape to the roughness amplitude has also been investigated. Then, the contribution rate of both fibre stiffness and tool feed has been quantified by the analysis of variance (ANOVA) at each analysis scale.

Multiscale mechanical structure of natural fibre composites

The natural fibres structure is extremely complex due to the hierarchical organization at different length scale and the different materials present in variable proportions.[17] The natural fibres used in the composites industry (Figure 1(a)) are in the form of bundles of elementary fibres (Figure 1(b)). Indeed, natural fibres are gathered in bundles of one to three dozen of elementary fibres and the bundle cohesion is insured by pectin interfaces.[18] Each elementary fibres is composed of concentric layers with different thicknesses, chemical compositions and structures (Figure 1(c)). The thin primary cell wall (P) coats the thicker secondary cell wall, which is responsible for the strength of the fibre. The

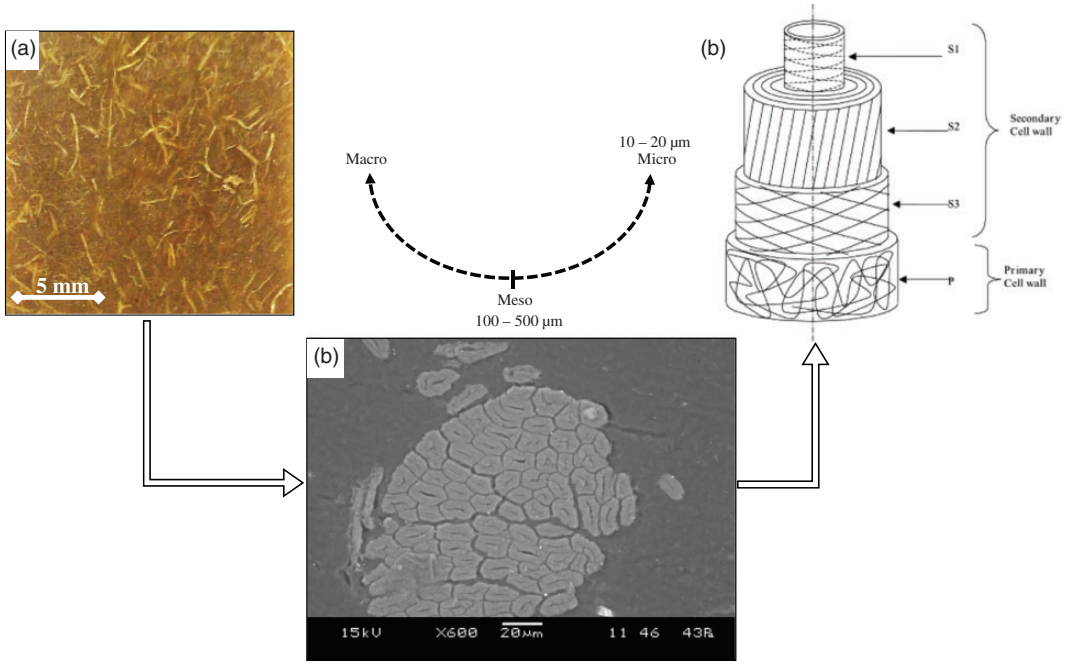

Figure 1. Multiscale NFRP structure. (a) Global sisal fibre/polypropylene structure. (b) Bundle structure of sisal fibres. (c) Schematization of elementary fibre structure.[17]

secondary cell wall encloses the lumen, which is a small channel in the middle that contributes to the water uptake. Each layer forms a micro-composite structure that is composed of microfibrils of cellulose embedded in amorphous matrix mainly made of pectin and hemicellulose.[19] The composition rates of these constituents are characterized by a high variability because of different natural factors such as the species and the variety of the plant, agricultural variables such as soil quality, the weathering conditions, the level of plant maturity and the quality of the retting process[17] in addition to the mechanical damages caused by the extraction step.[20] The bulk of the elementary fibre is essentially constituted by the layer (S2) of the secondary cell wall (Figure 1(c)). In S2, the microfibrils are displayed parallel one to another and form a microfibrilar angle with the fibre direction.[17]

Consequently, the machining study of NFRP cannot be conducted without taking into account the multiscale mechanical and physical structures involved at each characteristic scale.[21] At microscopic scale, the microfibrilar angle has an important effect on the mechanical behaviour of the natural elementary fibres. In fact, and unlike the linear glass fibre behaviour, Figure 2(a) shows a non-linear region in the earlier stage of the loading behaviour of natural fibres.[22] This non-linear behaviour is explained by the sliding of the microfibrils along with their progressive alignment with the fibre axis regarding the initial microfibrilar angle. This alignment would cause rearrangements in the core of the surrounding amorphous matrix, which would imply an elasto-visco-plastic deformation.[19,23] The behaviour becomes linear in the new rearrangement configuration. However, the natural fibre bundles, which refer to the mesoscopic scale, don't reveal the same behaviour as the elementary fibres that refer to the microscopic scale.[24] Indeed, the tensile test of natural fibre bundle shows a linear behaviour (Figure 2(b)). The non-linear behaviour revealed by the elementary fibres is not detected when the analysis takes into account all the elementary fibres grouped in the bundle. At macroscopic scale, the presence of the polymer matrix will induce an elasto-plastic behaviour[25] as shown in Figure 2(c). The mechanical strength decreases significantly between mesoscopic scale and macroscopic scale because of the low mechanical performances of the polymer matrix and the low adhesion between the natural fibre and polymer resin.[26]

This multiscale mechanical anisotropic behaviour will influence the machined surface when dry milling NFRP composites. Discrimination and correlations of these effects require:

- Characterizations of the machined surface at the appropriate scale;

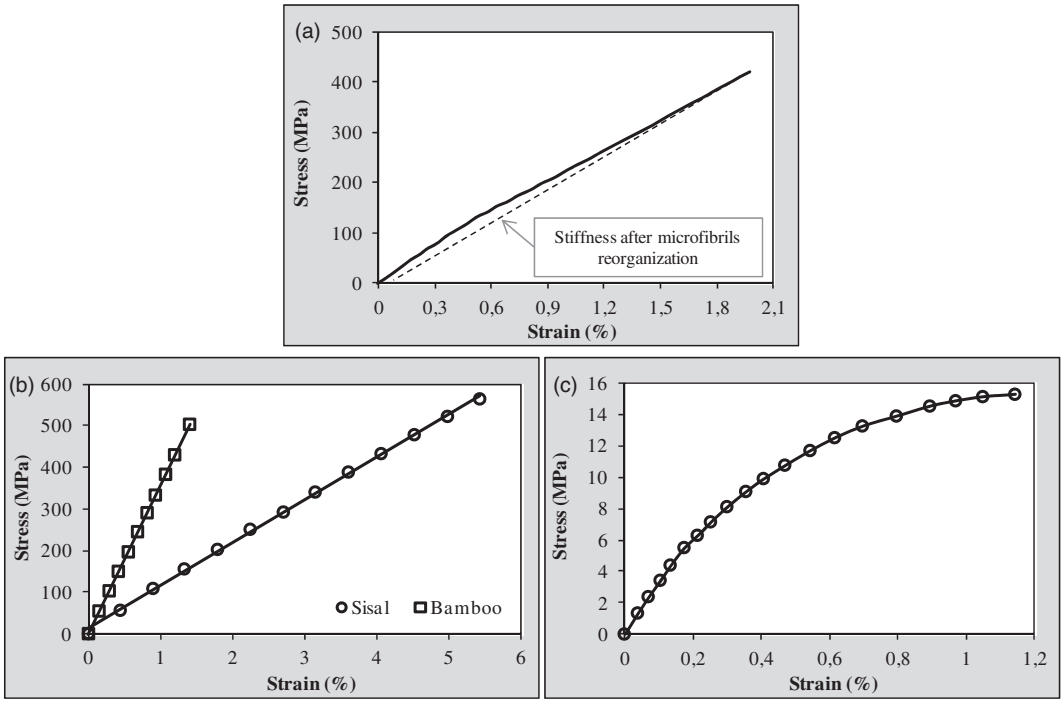

Figure 2. (a) Typical tensile behaviour of sisal elementary fibres.[22] (b) Typical tensile behaviour of bamboo and sisal fibre bundles.[24] (c) Typical tensile behaviour of bamboo reinforced polypropylene composite.[25]

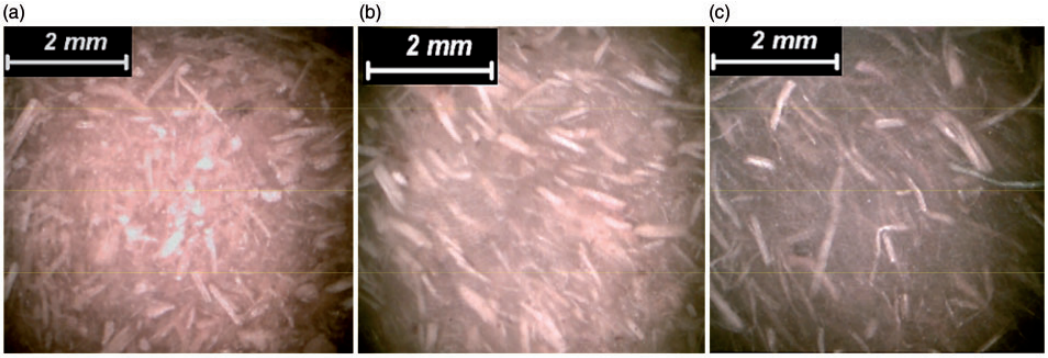

Figure 3. Optical microscope pictures of each specimen of NFRP showing randomly oriented short fibres. (a) PP/bamboo, (b) PP/miscanthus and (c) PP/sisal.

- Topographic measurements containing the appropriate scales with sufficient fidelity.

These requirements are developed in this work for milling NFRP composites using the approach of DWT and the ANOVA.

Experimental procedure

Three different natural fibres are considered in this study (Figure 3). Bamboo, sisal and miscanthus fibre are randomly oriented in workpiece samples and there lengths are about 1 mm. The samples are in form of rectangular plates of 2 mm of thickness and are prepared by injection moulding of polypropylene (PP) resin with the short randomly oriented fibres. Table 1 presents the mechanical characteristics provided by the supplier for each material in addition to the estimated fibre tensile modulus for each natural fibre, which are obtained by the rule of mixture of Halpin Tsai adapted by Nielson for randomly discontinuous fibre composites as explained in Chegdani et al.[16] Initial surface states were obtained by polishing the NFRP work-surfaces with the same grit size of sand paper before profile milling process. The polishing step was made in order to have the same initial surface state for all the studied workpieces.

Profile milling setup (Figure 4) was performed on instrumented DMU60 MonoBLOCK® five axes CNC machine. The milling tool chosen for this study is a helical carbide end mill of 12 mm of diameter and composed of two cutting edges with 25° of helix angle including polyglass flutes. Profile milling operations (Figure 5(a)) have been realized on dry cutting contact conditions varying the feed of milling tool. Being all other working parameters kept constant, three values of tool feed (f_z) have been considered. These values cover the suitable feed range for machining composite materials.[27] Table 2 summarizes the material/process parameters and variables used for profile milling tests.

Table 1. Mechanical properties of NFRP samples.

	PP/bamboo	PP/miscanthus	PP/sisal
Composite tensile modulus (MPa)	4100	2700	2200
Composite yield strength (MPa)	40	30	28
Estimated fibre tensile modulus (MPa)	19,000	13,800	7800

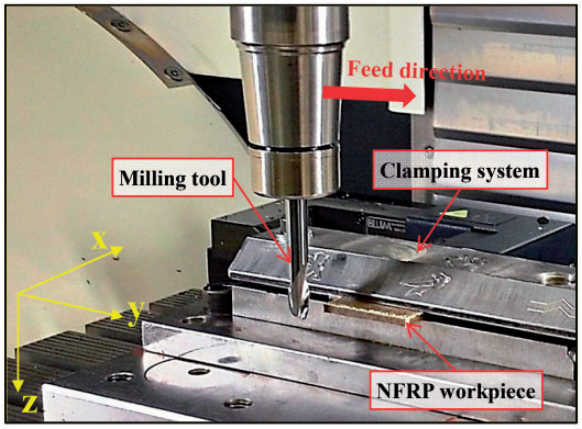

Figure 4. Profile milling setup on CNC machine.

Geometrical and superficial variations of each workpiece samples have been measured at five locations using a 2D Surfascan stylus profilometer (Figure 5(b)) according to the *ISO4287* standard in order to generate the topography signal of Figure 5(c). The tip radius of the diamond stylus is 2 µm. The surface micro-profile on each specimen was taken along the machining direction over a sampling length of 2 µm. The evaluation length is 16.8 mm and a cut-off of 0.8 mm is used to

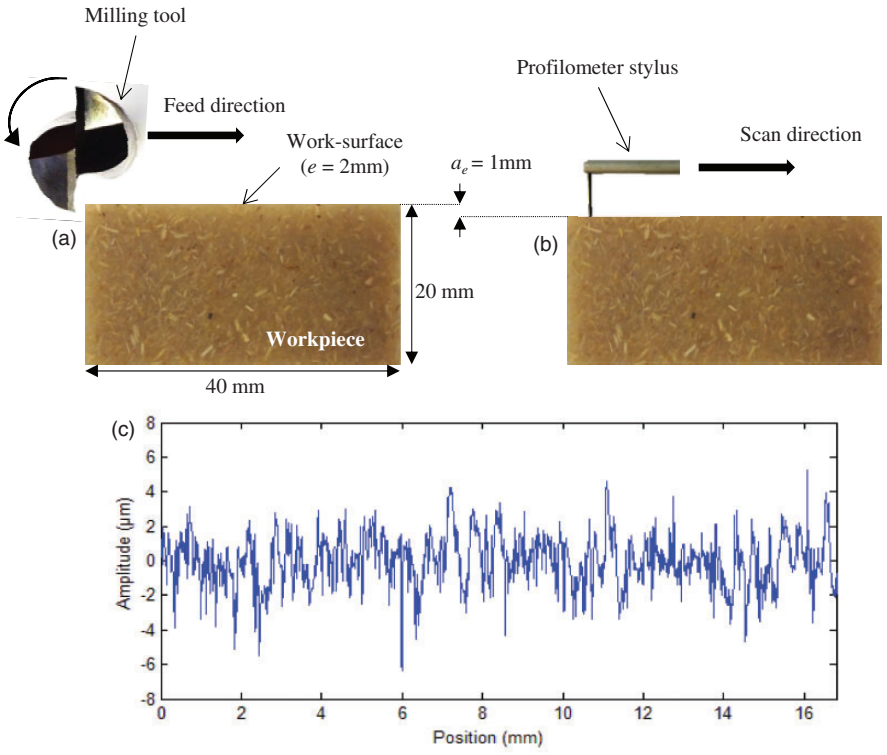

Figure 5. (a) Profile milling operation, (b) surface topography measurement and (c) typical machined surface topography signal for bamboo FRP at $f_z = 0.12$ mm/tooth.

Table 2. Material/process parameters used in the profile milling tests.

NFRP composite	Tool feed (mm/tooth)	Cutting speed (m/min)	Depth of cut (mm)
PP/bamboo	0.04		
PP/sisal	0.08	47	1
PP/miscanthus	0.12		

evaluate the arithmetic mean deviation of roughness (R_a) profile parameter. Each measurement has been performed before and after the profile milling tests.

Multiscale surface characterization using DWT

The geometrical surface structure in its longitudinal and lateral profiles contains complex characteristics of surface irregularities with roughness, waviness and shape components along the measured length. Material and process parameters impose characteristic irregularities on a part of the surface.[15] The objective of multiscale decomposition using wavelet approach is to find at which range, each material/process variable affects the morphology of the machined surface.

In fact, and unlike Fourier transform, which is limited by its fixed resolution in the space and frequency domains, the DWT[28–32] has a flexible time-frequency resolution by trading resolution in time for resolution in frequency.[10] DWT decomposes a signal into several sub-bands according to a recursive process. At each DWT decomposition, global topographic signal $f(x)$ (Figure 5(c)) processed through a series of high- and low-pass filters to analyse the high and low frequencies.[33] The down-sampled output of the high- and low-pass filters are respectively the detail and approximate wavelets coefficients. The procedure was then repeated for subsequent decompositions to achieve the desired level of the multi-resolution analysis. Then the wavelets coefficients were through synthesis filters to reconstruct the topographic signal at each decomposition levels.[16]

For DWT approach, the basis filtering functions are obtained from a single prototype wavelet, which called the 'Mother' wavelet '$\psi(x)$' by translation and dilation.[10] The general discretization of the wavelet as introduced by Daubechies[34] has the form:

$$\psi_{m,n}(x) = \frac{1}{\sqrt{a_0^m}} \left(\frac{x - nb_0 a_0^m}{a_0^m} \right) \quad (1)$$

where m and n are, respectively, the translation and dilation parameters.

The power-of-two logarithmic scaling of both the dilation and translation steps leads to the construction of an orthogonal wavelet basis ($a_0 = 2$ and $b_0 = 1$).

$$\text{Then :} \quad \psi_{m,n}(x) = 2^{-m/2}\psi(2^{-m}x - n) \tag{2}$$

The DWT of the signal $f(x)$ is defined by:

$$W(m,n) = \left\langle \overline{\psi}_{m,n}(x), f(x) \right\rangle \tag{3}$$

where $\overline{\psi}_{m,n}(x)$ is the conjugate of the wavelet function. The reconstruction of the initial signal $f(x)$ is then given by:

$$f(x) = \sum_{m,n} W(m,n)\psi_{m,n}(x) \tag{4}$$

Then, the multiscale transfer function of the morphological modification in machined surface after profile milling process, denoted by MPS, is determined.[35] It consists in calculating the arithmetic mean roughness (M_a) on each decomposition scale 'i' of the acquired roughness profile. Multiscale profile milling Process Signature ($MPS_{i)}$ is obtained by calculating the ratio of the equation (5). Where M_a^{init} and M_a^{fin} are the arithmetic mean roughness for the initial state and the after milling state, respectively. MPS quantifies the surface profile irregularities induced by profile milling process from microscopic scales to macroscopic scales depending on initial surface state and machining conditions.

$$MPS_i(\ \%) = \frac{M_a^{fin}(i) - M_a^{init}(i)}{M_a^{init}(i)} \times 100 \tag{5}$$

In this study, several discrete wavelet families and shapes are considered to analyse the effect of wavelet shape on the signal characterization (Table 3).

ANOVA

To quantify the effect of source factors (fibre stiffness, feed rate and wavelets shape) on the roughness level at each scale of the decomposition, mathematical models for profile milling of NFRP composites using regression analysis and the ANOVA[7,36] were elaborated. Linear regression analysis for the results of the MPS analysis was considered.

Sequential approach or Type I sum of squares was used to test main effects and interaction effects in ANOVA. It allows, first, to allocate the part of the explained variance to the main effects (one after the other), then to the two-way interaction(s) (one after the other) and then to increasingly higher order interactions if present.[37]

Experimental and predicted MPS_i signature responses are compared. The sum of squares (SS) and the fitted residual sum of squares (RSS) of these gaps are computed and collected from all the parallel models to form the predictive residual sum of squares (PRESS), which estimates the predictive ability of the model. The goodness-of-fit is evaluated for the considered model with the measure of the squared correlation coefficient (R^2) and the cross-validated squared correlation coefficient (Q^2).[38]

$$R^2 = 1 - \frac{RSS}{SS} \tag{6}$$

$$Q^2 = 1 - \frac{PRESS}{SS} \tag{7}$$

where R^2 is a real number between zero and one. A large value of R^2 indicates a better fitness of the model to the data. The predictive capability of a model is generally determined by Q^2, which is usually between zero and one. A higher Q^2 value indicates a more reliable model with excellent predictive power.[39] Q^2 can be negative for very poor models.

Finally, F-test[40] was used to quantify the significance of each input working factor 'α' by:

$$F(\alpha) = \frac{MS_{reg}(\alpha)}{MS_r} \tag{8}$$

where MS_{reg} is the mean square due to regression and MS_r is the residual mean square.

Table 3. Different wavelets used for the multiscale analysis.

Wavelet family	Order	Abbreviation
Daubechies	2, 4, 8, 16, 32	DB
Symlet	2, 4, 8, 16, 32	SYM
Coiflet	1, 2, 3, 4, 5	COIF
Biorthogonal	2.2, 2.4, 2.8	BIOR
Reverse biorthogonal	2.2, 2.4, 2.8	RBIO

Results and discussion

NFRP behaviour under milling and the effect on the machined surface morphology

In previous work of the authors,[16] it has been shown that the stiffest fibre (bamboo) shows the stiffest cutting contact and, then, the most efficient fibres shearing without significant debonding between fibres and polymer matrix (Figure 6). Indeed, in the contact between a rigid cutting tool and natural fibre, the energy can

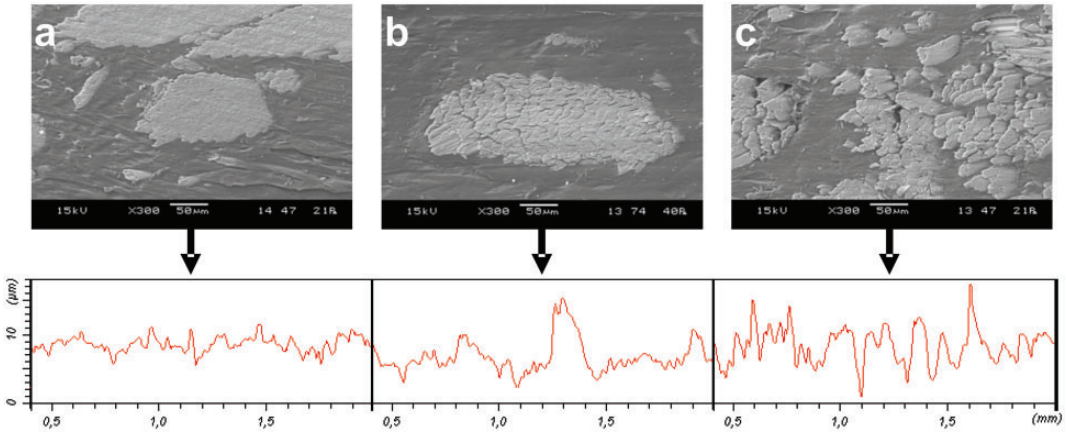

Figure 6. SEM observations and the corresponding topography signal of the milled surface for the three natural fibre composites. (a) PP/bamboo, (b) PP/miscanthus and (c) PP/sisal.

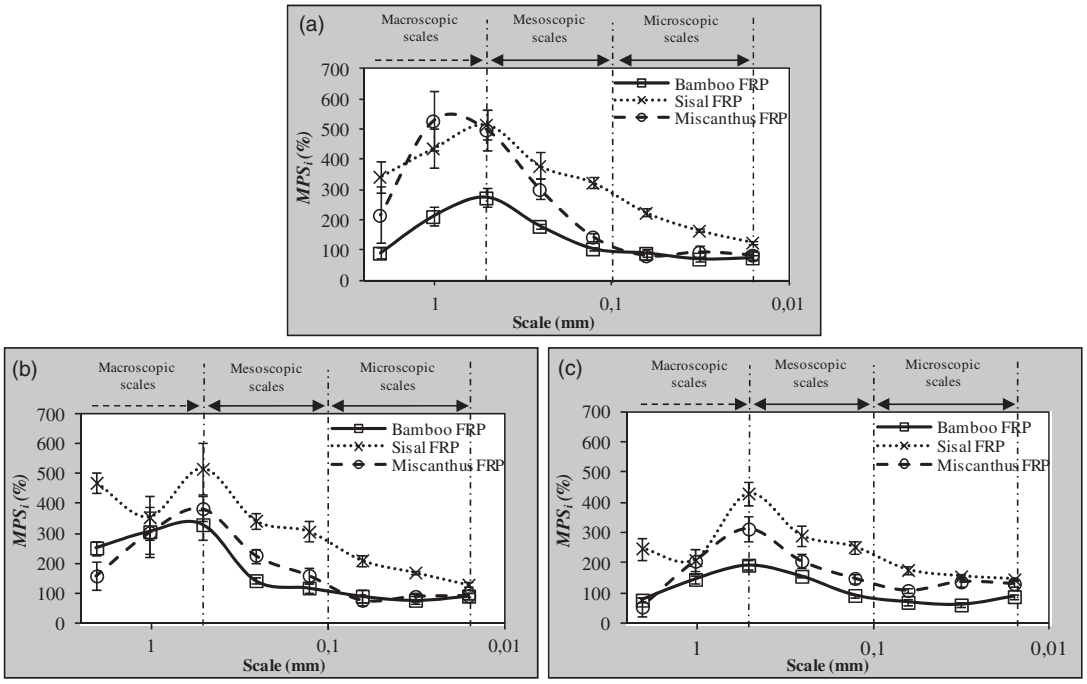

Figure 7. Multiscale profile milling process signature for the different NFRP at (a) $f_z = 0.04$ mm/tooth, (b) $f_z = 0.08$ mm/tooth and (c) $f_z = 0.12$ mm/tooth.

largely be dissipated through the deformation of the natural fibres[16,21] because of their high transversal flexibility induced by the natural cellulosic structure along the fibre axis.[17] The cross cut surface of the fibre does not show a ductile regime (pure shearing).[16] Consequently, both the exceeded uncut fibre extremities that remain on the milled surfaces and the debonding zones are the main responsible of the induced irregularities in the corresponding surface topography signal as shown in Figure 6. In the next sections, focus will be on the best way for analysing these surface topography signals.

Multiscale effect of milling feed and natural fibres on surface signal topography

Figure 7 presents the MPS of each NFRP for the different feed (f_z) values using a Coiflet wavelet of order 1 as analysis wavelet function. The MPS spectrums of each machined NFRP surface are composed of three

different behaviour areas, which can be related to three decomposition scale zones:

- Microscopic scales (10 and 100 μm): these represent the micro-roughness which is quasi-constant at all the microscopic scales range. The fibre type contribution to the roughness level is similar for both bamboo and miscanthus FRP at low and medium feed rates. We begin to see the difference of fibre type contribution at high feed rates from the higher scales of the microscopic zone.
- Mesoscopic scales (100 and 500 μm): this zone relates the scales which correspond to the natural fibre bundle section scales (Figure 1(b)). The impact of fibre type is significant on roughness contribution at this range of scales. Referring to the fibre stiffness values of Table 1, it reveals that the NFRP with the higher fibre stiffness has the low contribution to the roughness level. Increasing the tool feed participates to the reduction of the roughness signature at this range of scales.
- Macroscopic scales (>500 μm): These concern the scales which correspond to the global NFRP composite structure (Figure 1(a)). The contribution of all concerned NFRP to the roughness level decreases with the increasing of the tool feed. However, the impact of fibre type cannot be determined because of the randomly orientation of the short fibres within the composite.

The tool feed range (40, 80 and 120 μm) is located on the microscopic scale domain. The irregularities on the machined surface profile caused by changing the tool feed cannot be detected until reaching the scales that are higher than the tool feed range. Then, the tool feed effect on the MPS is not significant at the microscopic scales and start to be important at the beginning of the mesoscopic scales range.

The effect of fibre stiffness is dependent on the cutting scale. In fact, at microscopic scale, the cutting contact is between the cutting edge and the elementary fibre as shown in Figure 1(c). When the elementary fibre is mechanically solicited by the cutting edge, the interaction will induce the non-linear behaviour of the elementary fibre, which is produced by the sliding of the microfibrils along with their progressive alignment with the fibre axis as explained in 'Multiscale mechanical structure of natural fibre composites' section and Figure 2(a). Consequently, the tool/NFRP interaction at microscopic scale is not controlled by the stiffness of the microfibrils since they are not sufficiently aligned with the fibre axis and the fibre cut is produced before generating this alignment (i.e. the final linear behaviour of natural fibres shown in Figure 2(a)). At mesoscopic scale, the cutting contact is between the cutting edge and the fibre bundle as shown in Figure 1(b). At this range of scales, the cutting interaction will induce a linear behaviour controlled by the fibre bundle stiffness (Figure 2(b)). Thus, the fibre stiffness influences the cutting mechanism and, then, the surface quality. At macroscopic scale, the cutting contact is between the cutting edge and the global NFRP structure (Figure 1(a)). The cutting interaction will depend on the quantity of both fibre bundles and polymer matrix in contact with the cutting edge and hence the irregular behaviour of roughness signature at macroscopic scales.

Comparison with standard surface roughness analysis method

Standard surface roughness characterization had been performed by calculating the global roughness gain ratio (ΔR_a) between the mean roughness deviation of milled surface (R_a^{end}) and the mean roughness deviation of initial surface (R_a^{init}) using the following equation:

$$\Delta R_a(\ \%) = \frac{R_a^{end} - R_a^{init}}{R_a^{init}} \times 100 \tag{9}$$

In order to compare the standard and the multiscale surface roughness characterizations, the ΔR_a behaviour has been compared with the mean multiscale process signature (ΔMPS) behaviour at the mesoscopic scale range. Figure 8 presents the results for both ΔR_a and ΔMPS that have been drawn regarding the natural fibres stiffness of Table 1 for each milling feed values.

Globally, both standard and multiscale surface roughness methods show that profile milling process increases the surface roughness in comparison with the initial state. However, standard characterization (Figure 8(a)) indicates that increasing the tool feed (by a factor of 3) does not have a significant effect on the global surface roughness. Moreover, it does not show a difference in surface roughness level between bamboo and miscanthus fibres (i.e. fibre stiffness values of 19 and 13.8 GPa, respectively). On the other side, multiscale characterization (Figure 8(b)) reveals clearly that increasing the milling feed or the fibre stiffness decreases significantly the roughness level. Indeed, when increasing the tool feed, the chip thickness increases which satisfies the concept of the minimum chip thickness where the undeformed chip thickness is higher than the minimum chip thickness. This favours the shearing mechanism to adhesion or plastic deformation mechanisms.[21,41] Consequently, increasing the tool feed reduces the topographic irregularities and, then, reduces the surface roughness.

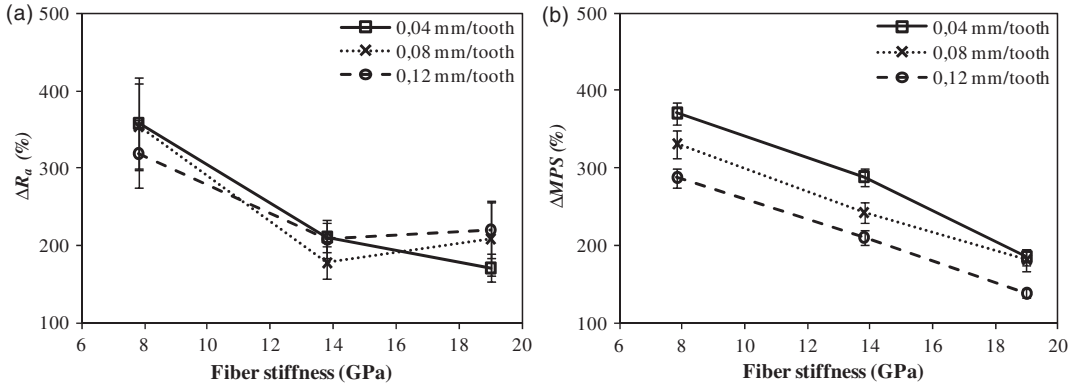

Figure 8. Comparison between (a) standard surface roughness analysis and (b) multiscale surface roughness analysis.

Consequently, the standard surface roughness analysis seems to be not able to identify the specific differences induced by the working parameters and the fibre properties on the milled surfaces. In other words, the standard R_a criterion on the global surface profile cannot discriminate the multiscale data in the initial signal topography (Figure 8(c)) of the machined surface profile.

Wavelets function choice: Influent variable or analysis noise?

By taking into account the standard deviation generated by the experimental measures, Figure 9 shows that the gap between average MPS signatures given by several wavelet types at mesoscopic scale for $i = 256\,\mu m$ (corresponding to the mean fibre bundle section diameter ($\sim$200 μm)) is not significant. Moreover, it can be noticed that some wavelet shapes are notable to well discriminate the natural fibre type effect on MPS at the same process conditions, especially at low and medium feed rate such as SYM4, RBIO2.2, RBIO2.4 at $f_z = 0.04\,mm/tooth$ and DB2, DB4, SYM2 at $f_z = 0.08\,mm/tooth$. It can be seen also that changing the wavelet type or wavelet order modifies the MPS amplitude for the same material/process condition. This effect is more obvious for sisal FRP because it generates the higher MPS values. Both Daubechies and Symlet wavelet families seem to have the same behaviour where changing the wavelet order. However, increasing the wavelet order does not have a regular influence on MPS response so it cannot be taken as an efficient criterion of choice for the wavelets function in the case of NFRP profile milling.

To statistically quantify the wavelet shape choice on the surface roughness response, two linear regression models have been constructed at first by XLSTAT software. The model 1 (M1) takes into account the variation of the wavelet shape as qualitative source variable. The model 2 (M2) takes into account the variation of the wavelet shape as a noise of analysis. Both M1 and M2 are a second-order linear regressions of MPS_i variables in terms of fibre tensile modulus and its square (E_f and E_f^2), feed rate and its square (f_z and f_z^2) in addition to the interaction between fibre tensile modulus and feed rate ($E_f \times f_z$) at each scale 'i' of the decomposition. MPS_i responses can then be expressed as a linear combination the previous factors. M1 and M2 models are evaluated with R^2 and Q^2 criteria in order to choose the most predictive model for the next ANOVA.

Figure 10 shows that Q^2 values are higher for M2 model at all the scales of the decomposition. Moreover, M2 exhibits equivalence between R^2 and Q^2 since they have closer values. According to the 'ANOVA' section, the model M2 is more predictive and it was chosen the next ANOVA studies. The wavelet's shape is then considered as a noise of analysis.

Contribution of fibre stiffness and feed factors on surface morphology signature

ANOVA of input variables influence has been performed at each MPS_i variable response (i.e. at each scale 'i' of the decomposition) using XLSTAT software as shown in Table 4. The P-value is computed assuming that the null 'α' factor hypothesis is true.[42] In other words, the P-value is computed based on the assumption that the 'α' source factor doesn't have a significant effect on the response.

ANOVA of the MPS responses shows that the order of each regression model depends on its decomposition scale 'i'. At microscopic scales, the model is a first-order regression since the F-test values of the second-order factors are too small compared with the F-test values of the first-order factors, and P-values of the second-order factors are too large compared with the P-values of the first-order factors. The significance of

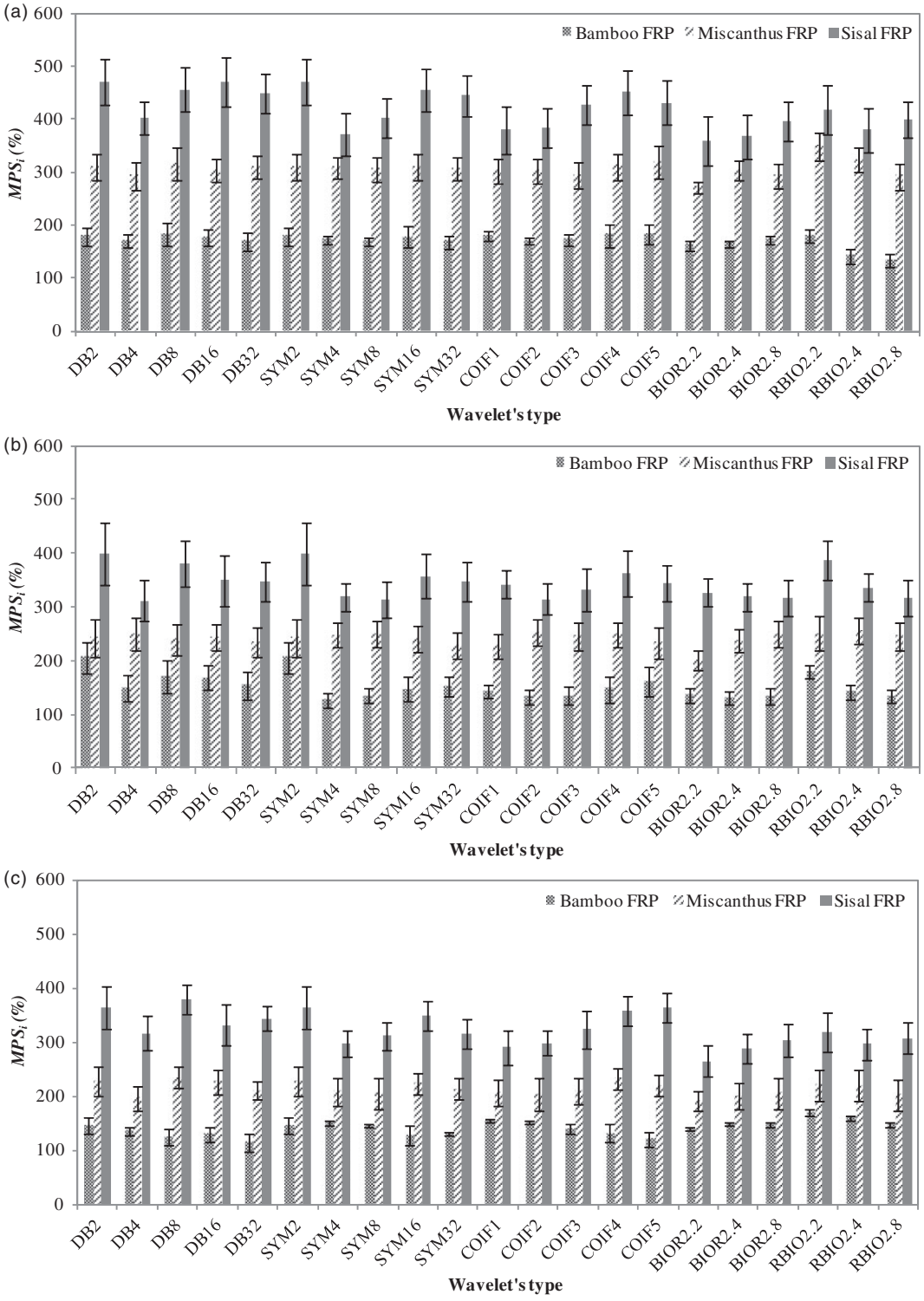

Figure 9. Multiscale profile milling process signature for the different NFRP by several wavelet types at the scale ix = 256 μm. (a) $f_z = 0.04$ mm/tooth, (b) $f_z = 0.08$ mm/tooth, (c) $f_z = 0.12$ mm/tooth.

the second-order factors begins to take effect from the scale $i = 0.064$ mm by the significance of E_f^2. The interaction effect starts to be significant from the mesoscopic scales ($i = 0.128$ mm).

To quantify the contribution significance of fibre stiffness factor, feed factor and the interaction, the contribution ratio of each 'α' factor ($C(\alpha)$) was calculated with the F-test at R^2 confidence.[7] It can be defined by

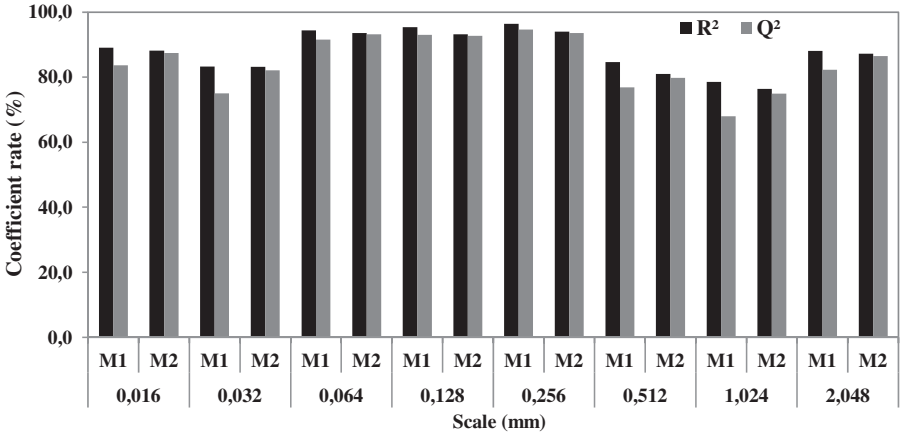

Figure 10. R^2 and Q^2 values for both M1 and M2 models at all the scales of the decomposition.

the following formula:

$$C(\alpha) = \frac{F(\alpha)}{\sum_{\alpha} F(\alpha)} \times R^2 \tag{10}$$

$$\text{Then} \quad \sum_{\alpha} C(\alpha) = R^2 \tag{11}$$

The contribution rate of both fibre stiffness and feed factors were obtained by summing the contribution rates of the first order and the second order of each factor:

$$C(\textit{fibre stiffness}) = C(E_f) + C\left(E_f^2\right) \tag{12}$$

$$\text{and} \quad C(\textit{feed}) = C(f_z) + C\left(f_z^2\right) \tag{13}$$

In order to compare the contribution rate criterion between the standard and the multiscale surface characterizations, ANOVA method has been identically applied to the results of the standard surface characterization presented in the Figure 8(a).

Figure 11 reveals that the contribution rates of natural fibre stiffness and feed factors are different at each analysis scale and present specific behaviours at three characteristic zones, which are closed to the characteristic zones defined by multiscale surface roughness analysis: At microscopic zone, fibre stiffness contribution increases significantly by scale increasing while feed contribution decreases significantly until becoming negligible. Interaction contribution is insignificant in this zone and also at mesoscopic scales. This second characteristic area indicates an opposite behaviour of the microscopic zone where fibre stiffness contribution decreases significantly by scale increasing while feed contribution increases by scale increasing. This behaviour is spread until the scale $i = 1$ mm, which shows the most significant contribution of the interaction between fibre stiffness and feed effects. Feed effect reaches its maximum and fibre stiffness effect reaches its minimum. After this scale, fibre stiffness contribution re-increases by scale increasing while feed contribution re-decreases by scale increasing at macroscopic scales.

Based on Figure 11, these differences in contribution rate behaviours at each characteristic scale area of multiscale decomposition can be physically explained by the nature of phases treated at each characteristic scale and the considered cutting scale. In fact, microscopic scales are within the fibre bundles. As explained in (NFRP behaviour under milling and the effect on the machined surface morphology) section, the feed effect is insignificant at microscopic scales and only the mechanical behaviour of elementary fibres is controlling the tool/material contact and surface roughness because the cutting contact scale includes only the elementary fibre. Thus, the fibre stiffness contribution rate increases by scale increasing, because it induced a growing of elementary fibre considered for the cutting contact and, then, the disappearance of the specific non-linear behaviour of natural elementary fibre. Mesoscopic scales correspond to the fibre bundle section diameters, which are between 100 μm and 500 μm. Feed contribution becomes significant as it controls the quantity of chopped fibres during the passage of the cutting edge. This contribution rate increases by scale increasing as explained in 'Multiscale effect of milling feed and natural fibres on surface signal topography' section and also because the probability of finding several fibre bundles will be more important. As consequence, the fibre stiffness contribution to the surface roughness decreases but it's still greater than the feed contribution until the scale $i = 1$ mm. Feed contribution

Table 4. ANOVA results for MPS analysis at each scale of the decomposition.

Source factor	DOF	SS	MS_{reg}	F-test	P-value
$i = 0.016$ mm ($R^2 = 88.2\%$)					
E_f	1	54,020.31	54,020.31	798.88	<0.0001
f_z	1	36,630.03	36,630.03	541.70	<0.0001
E_f^2	1	12.23	12.23	0.18	0.671
f_z^2	1	846.76	846.76	12.52	0.001
$E_f \times f_z$	1	860.39	860.39	12.72	0.001
$i = 0.032$ mm ($R^2 = 83.2\%$)					
E_f	1	175,334.47	175,334.47	888.73	<0.0001
f_z	1	2188.63	2188.63	11.09	0.001
E_f^2	1	637.14	637.14	3.23	0.074
f_z^2	1	48.30	48.30	0.24	0.621
$E_f \times f_z$	1	256.56	256.56	1.30	0.256
$i = 0.064$ mm ($R^2 = 93.6\%$)					
E_f	1	523,830.83	523,830.83	2376.65	<0.0001
f_z	1	1887.90	1887.90	8.56	0.004
E_f^2	1	59,820.85	59,820.85	271.41	<0.0001
f_z^2	1	1.23	1.23	0.006	0.940
$E_f \times f_z$	1	735.12	735.12	3.335	0.069
$i = 0.128$ mm ($R^2 = 93.2\%$)					
E_f	1	912,917.26	912,917.26	2195.31	<0.0001
f_z	1	13,319.69	13,319.69	32.03	<0.0001
E_f^2	1	86,522.70	86,522.70	208.06	<0.0001
f_z^2	1	14,496.51	14,496.51	34.86	<0.0001
$E_f \times f_z$	1	13,433.59	13,433.59	32.30	<0.0001
$i = 0.256$ mm ($R^2 = 94\%$)					
E_f	1	1,335,258.00	1,335,258.00	2486.76	<0.0001
f_z	1	174,514.60	174,514.60	325.01	<0.0001
E_f^2	1	136.95	136.95	0.25	0.614
f_z^2	1	12,839.04	12,839.04	23.91	<0.0001
$E_f \times f_z$	1	18,563.14	18,563.14	34.57	<0.0001
$i = 0.512$ mm ($R^2 = 81\%$)					
E_f	1	881,158.77	881,158.77	509.90	<0.0001
f_z	1	285,976.69	285,976.69	165.48	<0.0001
E_f^2	1	38,067.47	38,067.47	22.02	<0.0001
f_z^2	1	140,809.49	140,809.49	81.48	<0.0001
$E_f \times f_z$	1	3046.73	3046.73	1.76	0.186
$i = 1.024$ mm ($R^2 = 76.4\%$)					
E_f	1	462,998.96	462,998.96	101.12	<0.0001
f_z	1	1,707,738.93	1,707,738.93	372.99	<0.0001
E_f^2	1	347,147.16	347,147.16	75.82	<0.0001
f_z^2	1	368.50	368.50	0.08	0.777
$E_f \times f_z$	1	192,833.44	192,833.44	42.11	<0.0001
$i = 2.048$ mm ($R^2 = 87.2\%$)					
E_f	1	1,220,422.61	1,220,422.61	496.46	<0.0001
f_z	1	504,726.56	504,726.56	205.32	<0.0001
E_f^2	1	643,228.39	643,228.39	261.66	<0.0001
f_z^2	1	591,944.60	591,944.60	240.80	<0.0001
$E_f \times f_z$	1	111,464.89	111,464.89	45.34	<0.0001

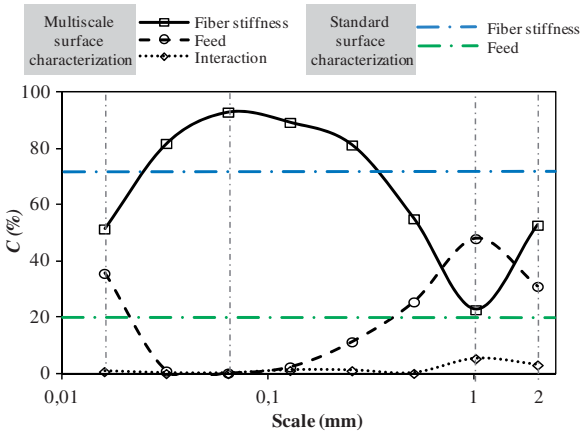

Figure 11. Contribution rate of fibre stiffness and tool feed at each scale of the NFRP composite surface topography.

becomes more important than fibre stiffness contribution, because the scale $i = 1$ mm is surely taking into account the macro-NFRP structure shown in Figure 1(a) with the elasto-plastic behaviour (Figure 2(c)). Consequently, the tool/material contact is more affected by the feed range than by the fibre stiffness variation because the cutting contact scale will include both natural fibre bundles and polymer matrix that reduce the material stiffness and, then, the contact stiffness. However, and after the scale $i = 1$ mm which corresponds to the mean fibre size as demonstrated by Chegdani et al.,[16] the random orientation of fibres comes into play and furthers, once again, the effect of the fibre stiffness. This behaviour is verified until the global surface roughness scale where fibre stiffness contribution is significantly more important than feed contribution. Indeed, the cutting scales higher than 1 mm are controlled by the mechanical behaviour of the macro-composite, whose mechanical properties are presented in Table 1. The difference in composites stiffness is due to the fibre stiffness since they have the same polymer matrix. Therefore, the macro-cutting scales are controlled by the fibre stiffness.

Conclusion

Multiscale decomposition approach by DWT has been operated in order to determine the MPS of profile milling process on NFRP composites. Several wavelet shapes has been tested and ANOVA method has been exploited to reveal the contribution rate of fibre stiffness and tool feed variables. The following conclusions have been revealed:

- Multiscale surface roughness analysis shows that the machined surface roughness behaviour of NFRP can be divided into three characteristic zones: microscopic

zone which corresponds to elementary fibre scales, mesoscopic zone which corresponds to the fibre bundle section scales and macroscopic zone which corresponds to the global composite scales.

- Wavelet shape has an insignificant effect on the discrimination quality of fibre type and tool feed effects in the multiscale NFRP surface roughness analysis. However, wavelet function variation has an impact on the MPS response at high roughness levels. Thus, wavelet variation can be considered as a noise of MPS analysis.
- The ANOVA applied to the multiscale analysis results shows that the contribution rates of both fibre stiffness and tool feed to the surface roughness modification after milling depend strongly on the analysis scale. The contribution rates of fibre stiffness and milling feed on the machined NFRP surfaces are revealed at separated characteristic scales range.
- This study demonstrates that the multiscale topographic behaviour of machined surface signals is related to the mechanical behaviour of the materials that are inside the considered analysis scale.

Acknowledgements

The authors wish to thank '*AD majoris SAS France*' for providing the NFRP samples used in this research.

Declaration of Conflicting Interests

The author(s) declared no potential conflicts of interest with respect to the research, authorship, and/or publication of this article.

Funding

The author(s) disclosed receipt of the following financial support for the research, authorship, and/or publication of this article: Urban community of Châlons-en-Champagne (*Cités en Champagne*).

References

1. Faruk O, Bledzki AK, Fink H-P, et al. Biocomposites reinforced with natural fibers: 2000–2010. *Prog Polym Sci* 2012; 37: 1552–1596.
2. Dittenber DB and GangaRao HVS. Critical review of recent publications on use of natural composites in infrastructure. *Compos A: Appl Sci Manuf* 2012; 43: 1419–1429.
3. Shah DU. Developing plant fibre composites for structural applications by optimising composite parameters: a critical review. *J Mater Sci* 2013; 48: 6083–6107.
4. Sakthivel M, Vijayakumar S and Ramesh S. Production and characterization of luffa/coir reinforced polypropylene composite. *Procedia Mater Sci* 2014; 5: 739–745.
5. Shalwan A and Yousif BF. In State of Art: Mechanical and tribological behaviour of polymeric composites based on natural fibres. *Mater Des* 2013; 48: 14–24.
6. Lefeuvre A, Bourmaud A, Morvan C, et al. Tensile properties of elementary fibres of flax and glass: Analysis of reproducibility and scattering. *Mater Lett* 2014; 130: 289–291.
7. Davim JP and Reis P. Damage and dimensional precision on milling carbon fiber-reinforced plastics using design experiments. *J Mater Process Technol* 2005; 160: 160–167.
8. Landon Y and Cherif M. Characterization of the surface quality of holes drilled in CFRP laminates. *Advanced Materials Research* 2013; 698: 107–116. DOI: 10.4028/www.scientific.net/AMR.698.107.
9. Lee S-H, Zahouani H, Caterini R, et al. Morphological characterisation of engineered surfaces by wavelet transform. *Int J Mach Tools Manuf* 1998; 38: 581–589.
10. Chen X, Raja J and Simanapalli S. Multi-scale analysis of engineering surfaces. *Int J Mach Tools Manuf* 1995; 35: 231–238.
11. El Mansori M, Mezghani S, Sabri L, et al. On concept of process signature in analysis of multistage surface formation. *Surf Eng* 2010; 26: 216–223.
12. Le Goïc G, Bigerelle M, Samper S, et al. Multiscale roughness analysis of engineering surfaces: A comparison of methods for the investigation of functional correlations. *Mech Syst Signal Process* 2016; 66–67: 437–457.
13. Ahuja N, Lertrattanapanich S and Bose NK. Properties determining choice of mother wavelet. *IEE Proceedings – Vision, Image, and Signal Processing* 2005; 152: 659–664. DOI: 10.1049/ip-vis:20045034.
14. Mezghani S, Sabri L, El Mansori M, et al. On the optimal choice of wavelet function for multiscale honed surface characterization. *J Phys Conf Ser* 2011; 311: 12025.
15. Bigerelle M, Guillemot G, Khawaja Z, et al. Relevance of Wavelet Shape Selection in a complex signal. *Mech Syst Signal Process* 2013; 41: 14–33.
16. Chegdani F, Mezghani S, El Mansori M, et al. Fiber type effect on tribological behavior when cutting natural fiber reinforced plastics. *Wear* 2015; 332–333: 772–779.
17. Baley C. Analysis of the flax fibres tensile behaviour and analysis of the tensile stiffness increase. *Compos A: Appl Sci Manuf* 2002; 33: 939–948.
18. Morvan C, Andème-Onzighi C, Girault R, et al. Building flax fibres: more than one brick in the walls. *Plant Physiol Biochem* 2003; 41: 935–944.
19. Charlet K, Baley C, Morvan C, et al. Characteristics of Hermès flax fibres as a function of their location in the stem and properties of the derived unidirectional composites. *Compos A: Appl Sci Manuf* 2007; 38: 1912–1921.
20. Van de Weyenberg I, Ivens J, De Coster A, et al. Influence of processing and chemical treatment of flax fibres on their composites. *Compos Sci Technol* 2003; 63: 1241–1246.
21. Chegdani F, Mezghani S and El Mansori M. Experimental study of coated tools effects in dry cutting of natural fiber reinforced plastics. *Surf Coatings Technol* 2015; 284: 264–272.
22. Silva FDA, Chawla N and Filho RDDT. Tensile behavior of high performance natural (sisal) fibers. *Compos Sci Technol* 2008; 68: 3438–3443.

23. Marrot L, Lefeuvre A, Pontoire B, et al. Analysis of the hemp fiber mechanical properties and their scattering (Fedora 17). *Ind Crops Prod* 2013; 51: 317–327.
24. Rao KMM and Rao KM. Extraction and tensile properties of natural fibers: Vakka, date and bamboo. *Compos Struct* 2007; 77: 288–295.
25. Chen X, Guo Q and Mi Y. Bamboo fiber-reinforced polypropylene composites: A study of the mechanical properties. *J Appl Polym Sci* 1998; 69: 1891–1899.
26. Li X, Tabil LG and Panigrahi S. Chemical treatments of natural fiber for use in natural fiber-reinforced composites: A review. *J Polym Environ* 2007; 15: 25–33.
27. Ben Soussia A, Mkaddem A and El Mansori M. Rigorous treatment of dry cutting of FRP – Interface consumption concept: A review. *Int J Mech Sci* 2014; 83: 1–29.
28. Qiu Z, Lee C-M, Xu ZH, et al. A multi-resolution filtered-x LMS algorithm based on discrete wavelet transform for active noise control. *Mech Syst Signal Process* 2016; 66–67: 458–469.
29. Peng ZK, Jackson MR, Rongong JA, et al. On the energy leakage of discrete wavelet transform. *Mech Syst Signal Process* 2009; 23: 330–343.
30. Chen B, Zhang Z, Sun C, et al. Fault feature extraction of gearbox by using overcomplete rational dilation discrete wavelet transform on signals measured from vibration sensors. *Mech Syst Signal Process* 2012; 33: 275–298.
31. Katunin A. Damage identification in composite plates using two-dimensional B-spline wavelets. *Mech Syst Signal Process* 2011; 25: 3153–3167.
32. Dick AJ, Phan QM, Foley JR, et al. Calculating scaling function coefficients from system response data for new discrete wavelet families. *Mech Syst Signal Process* 2012; 27: 362–369.
33. Chowdhury SK, Nimbarte AD, Jaridi M, et al. Discrete wavelet transform analysis of surface electromyography for the fatigue assessment of neck and shoulder muscles. *J Electromyogr Kinesiol* 2013; 23: 995–1003.
34. Daubechies I. *Ten lectures on wavelets*. Philadelphia: Society for Industrial and Applied Mathematics, 1992.
35. Mezghani S, El Mansori M, Massaq A, et al. Correlation between surface topography and tribological mechanisms of the belt-finishing process using multiscale finishing process signature. *Comptes Rendus Mécanique* 2008; 336: 794–799.
36. Gonsalez CG, da Silva S, Brennan MJ, et al. Structural damage detection in an aeronautical panel using analysis of variance. *Mech Syst Signal Process* 2015; 52–53: 206–216.
37. Kherad-Pajouh S and Renaud O. An exact permutation method for testing any effect in balanced and unbalanced fixed effect ANOVA. *Comput Stat Data Anal* 2010; 54: 1881–1893.
38. Wold S, Sjöström M and Eriksson L. PLS-regression: a basic tool of chemometrics. *Chemom Intell Lab Syst* 2001; 58: 109–130.
39. Wang H, Shangguan L, Wu J, et al. Multiple linear regression modeling for compositional data. *Neurocomputing* 2013; 122: 490–500.
40. Massart DL, Vandeginste BG, Buydens LMC, et al. *Handbook of Chemometrics and Qualimetrics: Part A*. Amsterdam: Elsevier B.V., 1998.
41. Chae J, Park SS and Freiheit T. Investigation of micro-cutting operations. *Int J Mach Tools Manuf* 2006; 46: 313–332.
42. Kline RB. *Beyond significance testing: Reforming data analysis methods in behavioral research,* 10.1037/10693-000\n, http://search.ebscohost.com/login.aspx?direct=true&db=pzh&AN=2004-13019-000&site=ehost-live (2004, accessed 18 October 2016).